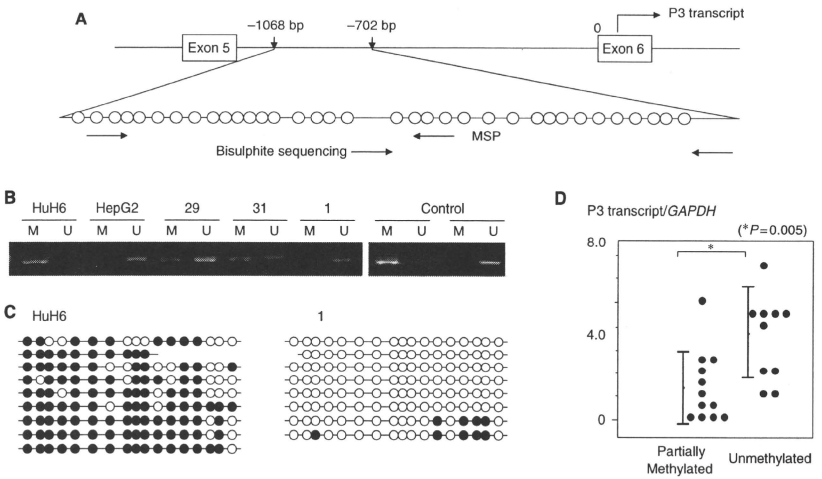

Figure 4 (**A**) Diagram of the *IGF2* P3 promoter region. Individual CpG dinucleotides located upstream of exon 6 (from −1068 to −702 bp) are represented by circles. Horizontal arrows indicate locations of PCR primers used for MSP and bisulphite sequencing. (**B**) Examples of the promoter methylation status using methylation-specific PCR. Polymerase chain reaction products of methylated or unmethylated P3 promoters from HB tumours are shown. Numbers above horizontal bars indicate the tumour number. M, methylated promoter; U, unmethylated promoter. (**C**) Bisulphite sequencing analysis of the methylation status of P3 promoter in HuH6 and one tumour (no. 1), which displayed complete methylation and complete unmethylation, respectively. Open and closed circles indicate unmethylated and methylated CpG dinucleotides, respectively. (**D**) Levels of P3 transcripts in tumours with partially methylated P3 promoter and tumours with unmethylated P3 promoter.

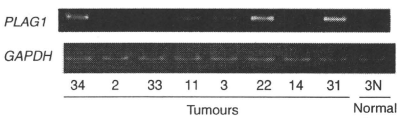

Figure 5 Representative data of RT–PCR analysis of *PLAG1* mRNA. Numbers below lanes indicate the tumour number.

et al, 2008), indicating that embryonal kidney tissues might be more susceptible to IGF2 stimulation than embryonal liver tissues. These findings might be related to higher incidences of UPD or LOI in WT than in HB.

The *IGF2* gene has four promoter regions and each promoter can initiate transcription producing a distinct *IGF2* transcript with different 5′-untranslated regions with a common translated region in the 3′-side (Li *et al*, 1998a). The *IGF2* gene is transcriptionally regulated in a development-dependent and tissue-specific manner. In the foetal liver, promoters P2, P3, and P4 are active and expressed monoallelically; P3 is the most active promoter and P1 is inactive. However, in the adult liver, P1 becomes dominant and is biallelically expressed, and P2, P3 and P4 activities are decreased or lost (Li *et al*, 1998a). In foetal liver tissues, P3 promoter methylation is inversely correlated with the P3 transcript expression. The inverse correlation between P3 promoter methylation and P3 transcript expression was reported earlier in seven HB tumours (Li *et al*, 1998b). This study confirmed the upregulation of P2, P3 and P4 transcripts and downregulation of P1 transcript, and

Table 2 Incidences of LOH of *IGF2* in previous and present series of hepatoblastoma and Wilms' tumours

References	Total number	LOH of *IGF2*[a]	No-LOH of *IGF2*	%
Hepatoblastoma				
Montagna *et al* (1994)	13	3	10	23.1
Fukuzawa *et al* (1999)	7	2	5	28.6
Gray *et al* (2000)	10	2	8	20.0
Hartmann *et al* (2000)	24	6	18	25.0
Albrecht *et al* (2004)	56	13	43	23.2
Suzuki *et al* (2008)	17	4	13	23.5
Total number	127	30	97	23.6
Present study	54	12	42	22.2
Wilms' tumour				
Grundy *et al* (1996)	260	93	167	35.8
Yuan *et al* (2005)	62	26	36	41.9

[a]Tumours with LOH of 11p15, but no informative *IGF2* locus are included.

the inverse correlation between P3 promoter methylation and P3 transcript expression in the majority of 20 HB tumours. Although P2, P3 and P4 transcripts were all correlated to the total amount of *IGF2* mRNAs, the earlier and present studies showed that the P3 transcript was most abundant and seemed to play a major role in the tumorigenesis of HB (Li *et al*, 1998b). Increased *IGF2* expression with the predominant P3 transcript was reported earlier in WTs with LOI or ROI (Vu and Hoffman, 1999). This study also showed that HB tumours with hypermethylated *H19* DMR tended to have an unmethylated P3 promoter, indicating that

Table 3 Incidences of LOI of *IGF2* in previous and present series of hepatoblastoma and Wilms' tumours

References	Total number[a]	LOI of *IGF2*	ROI of *IGF2*	%
Hepatoblastoma				
Davies (1993)	3	0	3	0
Montagna *et al* (1994)	5	1	4	20.0
Rainier *et al* (1995)	5	1	4	20.0
Li *et al* (1995)	3	1	2	33.3
Fukuzawa *et al* (1999)	4	1	3	25.0
Ross *et al* (2000)	13	3	10	23.1
Hartmann *et al* (2000)	5	3	2	60.0
Total number	38	10	28	26.3
Present study	42	9	33	21.4
Wilms' tumour				
Ravenel *et al* (2001)	36	15	21	41.7
Yuan *et al* (2005)	29	22	7	75.9

[a]Tumours with LOH of *IGF2* were excluded.

Table 4 Incidences of LOH, LOI and ROI of *IGF2* in hepatoblastoma and Wilms' tumours

References	Total number	LOH of *IGF2*	LOI of *IGF2*	ROI of *IGF2*
Hepatoblastoma				
Present study	54	12 (22.2%)	9 (16.7%)	33 (61.1%)
Wilms' tumour				
Fukuzawa *et al* (2004)	41	17 (41.5%)	13 (31.7%)	11 (26.8%)
Yuan *et al* (2005)	58	29 (50.0%)	22 (37.9%)	7 (12.1%)

the paternal P3 promoter or the maternal P3 promoter upstream of the aberrantly methylated *H19* DMR is likely to be unmethylated, probably because of stimulation of the enhancer signal. In contrast, the significance of unmethylation in the P3 promoter found in 4 (nos. 23, 24, 26 and 27) of 13 HB tumours with normally methylated *H19* DMR (ROI) remains unresolved.

PLAG1 located in 8q11 encodes a developmentally regulated transcription factor, and positively regulates *IGF2*. The P3 promoter region of *IGF2* contains *PLAG1* consensus-binding sites, and PLAG1 transactivates the transcription from embryonic *IGF2* promoter P3 in HB cell lines, HuH6 and HepG2 (Zatkova *et al*, 2004). *PLAG1* mRNA was highly expressed in most HB tumours compared with normal liver tissues. In this study, HB tumours with *PLAG1* mRNA expression showed and tended to show higher levels of P4 and P3 transcripts, respectively. Thus, the correlation of *PLAG1* mRNA expression with increased levels of P3 transcripts reported by Zatkova *et al* (2004) may be confirmed; furthermore, the correlation of *PLAG1* mRNA expression with increased levels of P4 transcripts was also suggested.

WTs can be classified at least into two groups; one has intralobar nephrogenic rest that is associated with *WT1* abnormality and the other has perilobar nephrogenic rest associated with *IGF2*-LOI (Ravenel *et al*, 2001). *CTNNB1* mutation is frequently found in WTs with *WT1* abnormality, but rare in WTs without *WT1* abnormality (Maiti *et al*, 2000). These findings suggest that WTs with no *WT1* abnormality may include a substantial number of tumours with *IGF2*-LOI, and that *CTNNB1* mutation and *IGF2*-LOI may be mutually exclusive in WT and also in HB. However, there were no differences in the incidences of *CTNNB1* mutation between HBs with *IGF2*-LOI and those with *IGF2*-ROI, or those with *IGF2*-LOH. We have recently reported a paper describing the occurrence of duplication of paternal *IGF2* or *IGF2*-LOI in half of WTs with *WT1* abnormalities (Haruta *et al*, 2008). Of two WTs with *IGF2*-LOI and *WT1* abnormality reported in that paper, one had *CTNNB1* mutation and the other had not. These findings suggest that *CTNNB1* mutation and *IGF2*-LOI may not be mutually exclusive in either WT or HB.

The IGF signalling pathway is activated in various cancers, and monoclonal antibodies targeting IGF1R have been recently developed; IGF1R is a transmembrane tyrosine kinase receptor, and both IGF1 and IGF2 are ligands for IGF1R (Foulstone *et al*, 2005). Early clinical trials using anti-IGF1R monoclonal antibodies showed promising results in refractory Ewing's sarcomas and rhabdomyosarcomas (Ryan and Goss, 2008). Because 20–30% of HB tumours do not respond to the current chemotherapy consisting of cisplatin and adriamycin (Perilongo *et al*, 2000; Fuchs *et al*, 2002), and the great majority of HB tumours overexpresses *IGF2*, as shown in the present and earlier studies, HB may be the next target tumour for antibody therapy.

ACKNOWLEDGEMENTS

This study was supported by Ministry of Health, Labor and Welfare, Japan for Third-Term Comprehensive Control Research for Cancer (Y Kaneko). We are grateful to Dr K Hiyama, Hiroshima University, a data administrator for JPLT, for data management. We also express our gratitude to the physicians participating in JPLT who supplied samples for this study.

REFERENCES

Albrecht S, Hartmann W, Houshdaran F, Koch A, Gärtner B, Prawitt D, Zabel BU, Russo P, Von Schweinitz D, Pietsch T (2004) Allelic loss but absence of mutations in the polyspecific transporter gene *BWR1A* on 11p15.5 in hepatoblastoma. *Int J Cancer* **111:** 627–632

Beeghly AC, Katsaros D, Wiley AL, Rigault de la Longrais IA, Prescott AT, Chen H, Puopolo M, Rutherford TJ, Yu H (2007) IGF-II promoter methylation and ovarian cancer prognosis. *J Cancer Res Clin Oncol* **133:** 713–723

Bell AC, Felsenfeld G (2000) Methylation of a CTCF-dependent boundary controls imprinted expression of the *Igf2* gene. *Nature* **405:** 482–485

Davies SM (1993) Maintenance of genomic imprinting at the IGF2 locus in hepatoblastoma. *Cancer Res* **53:** 4781–4783

Foulstone E, Prince S, Zaccheo O, Burns JL, Harper J, Jacobs C, Church D, Hassan AB (2005) Insulin-like growth factor ligands, receptors, and binding proteins in cancer. *J Pathol* **205:** 145–153

Fuchs J, Rydzynski J, Von Schweinitz D, Bode U, Hecker H, Weinel P, Bürger D, Harms D, Erttmann R, Oldhafer K, Mildenberger H (2002) Pretreatment prognostic factors and treatment results in children with hepatoblastoma. *Cancer* **95:** 172–182

Fukuzawa R, Breslow NE, Morison IM, Dwyer P, Kusafuka T, Kobayashi Y, Becroft DM, Beckwith JB, Perlman EJ, Reeve AE (2004) Epigenetic differences between Wilms' tumours in white and East-Asian children. *Lancet* **363:** 446–451

Fukuzawa R, Umezawa A, Ochi K, Urano F, Ikeda H, Hata J (1999) High frequency of inactivation of the imprinted *H19* gene in 'sporadic' hepatoblastoma. *Int J Cancer* **82:** 490–497

Gray SG, Eriksson T, Ekström C, Holm S, von Schweinitz D, Kogner P, Sandstedt B, Pietsch T, Ekström TJ (2000) Altered expression of members of the IGF-axis in hepatoblastomas. *Br J Cancer* **82:** 1561–1567

Grundy P, Telzerow P, Moksness J, Breslow NE (1996) Clinicopathologic correlates of loss of heterozygosity in Wilms' tumors: a preliminary analysis. *Med Pediatr Oncol* **27:** 429–433

Hark AT, Schoenherr CJ, Katz DJ, Ingram RS, Levorse JM, Tilghman SM (2000) CTCF mediates methylation-sensitive enhancer-blocking activity at the *H19/Igf2* locus. *Nature* **405:** 486–489

Hartmann W, Waha A, Koch A, Goodyer CG, Albrecht S, von Schweinitz D, Pietsch T (2000) $p57^{KIP2}$ is not mutated in hepatoblastoma but shows increased transcriptional activity in a comparative analysis of the three imprinted genes $p57^{KIP2}$, *IGF2*, and *H19*. *Am J Pathol* **157:** 1393–1403

Haruta M, Arai Y, Sugawara W, Watanabe N, Honda S, Ohshima J, Soejima H, Nakadate H, Okita H, Hata J, Fukuzawa M, Kaneko Y (2008) Duplication of paternal *IGF2* or loss of maternal *IGF2* imprinting occurs in half of Wilms tumors with various structural *WT1* abnormalities. *Genes Chromosomes Cancer* **47:** 712–727

Hedborg F, Holmgren L, Sandstedt B, Ohlsson R (1994) The cell type-specific *IGF2* expression during early human development correlates to the pattern of overgrowth and neoplasia in the Beckwith–Wiedemann syndrome. *Am J Pathol* **145:** 802–817

Herman JG, Graff JR, Myöhänen S, Nelkin BD, Baylin SB (1996) Methylation-specific PCR: a novel PCR assay for methylation status of CpG islands. *Proc Natl Acad Sci USA* **93:** 9821–9826

Honda S, Haruta M, Sugawara W, Sasaki F, Ohira M, Matsunaga T, Yamaoka H, Horie H, Ohnuma N, Nakagawara A, Hiyama E, Todo S, Kaneko Y (2008) The methylation status of *RASSF1A* promoter predicts responsiveness to chemotherapy and eventual cure in hepatoblastoma patients. *Int J Cancer* **123:** 1117–1125

Koch A, Denkhaus D, Albrecht S, Leuschner I, Von Schweinitz D, Pietsch T (1999) Childhood hepatoblastomas frequently carry a mutated degradation targeting box of the β-catenin gene. *Cancer Res* **59:** 269–273

Li X, Adam G, Cui H, Sandstedt B, Ohlsson R, Ekström TJ (1995) Expression, promoter usage and parental imprinting status of insulin-like growth factor II (*IGF2*) in human hepatoblastoma: uncoupling of *IGF2* and *H19* imprinting. *Oncogene* **11:** 221–229

Li X, Gray SG, Flam F, Pietsch T, Ekström TJ (1998a) Developmental-dependent DNA methylation of the *IGF2* and *H19* promoters is correlated to the promoter activities in human liver development. *Int J Dev Biol* **42:** 687–693

Li X, Kogner P, Sandstedt B, Haas OA, Ekström TJ (1998b) Promoter-specific methylation and expression alterations of *igf2* and *h19* are involved in human hepatoblastoma. *Int J Cancer* **75:** 176–180

Lu L, Katsaros D, Wiley A, Rigault de la Longrais IA, Puopolo M, Schwartz P, Yu H (2006) Promoter-specific transcription of insulin-like growth factor II in epithelial ovarian cancer. *Gynecol Oncol* **103:** 990–995

Maiti S, Alam R, Amos CI, Huff V (2000) Frequent association of β-*catenin* and *WT1* mutations in Wilms tumors. *Cancer Res* **60:** 6288–6292

Matsunaga T, Sasaki F, Ohira M, Hashizume K, Hayashi A, Hayashi Y, Matsuyama K, Mugishima H, Ohnuma N (2004) The role of surgery in the multimodal treatment for hepatoblastomas. *Shounigan* **41:** 205–210 (in Japanese)

Montagna M, Menin C, Chieco-Bianchi L, D'Andrea E (1994) Occasional loss of constitutive heterozygosity at 11p15.5 and imprinting relaxation of the *IGFII* maternal allele in hepatoblastoma. *J Cancer Res Clin Oncol* **120:** 732–736

Perilongo G, Shafford EA (1999) Liver tumours. *Eur J Cancer* **35:** 953–958

Perilongo G, Shafford S, Plaschkes J (2000) SIOPEL trials using preoperative chemotherapy in hepatoblastoma. *Lancet Oncol* **1:** 94–100

Rainier S, Dobry CJ, Feinberg AP (1995) Loss of imprinting in hepatoblastoma. *Cancer Res* **55:** 1836–1838

Ravenel JD, Broman KW, Perlman EJ, Niemitz EL, Jayawardena TM, Bell DW, Haber DA, Uejima H, Feinberg AP (2001) Loss of imprinting of insulin-like growth factor-II (IGF2) gene in distinguishing specific biologic subtypes of Wilms tumor. *J Natl Cancer Inst* **93:** 1698–1703

Ross JA, Radloff GA, Davies SM (2000) *H19* and *IGF-2* allele-specific expression in hepatoblastoma. *Br J Cancer* **82:** 753–756

Ryan PD, Goss PE (2008) The emerging role of the insulin-like growth factor pathway as a therapeutic target in cancer. *Oncologist* **13:** 16–24

Satoh Y, Nakagawachi T, Nakadate H, Kaneko Y, Masaki Z, Mukai T, Soejima H (2003) Significant reduction of *WT1* gene expression, possibly due to epigenetic alteration in Wilms' tumor. *J Biochem* **133:** 303–308

Steenman MJ, Rainier S, Dobry CJ, Grundy P, Horon IL, Feinberg AP (1994) Loss of imprinting of *IGF2* is linked to reduced expression and abnormal methylation of *H19* in Wilms tumor. *Nat Genet* **7:** 433–439

Sugawara W, Haruta M, Sasaki F, Watanabe N, Tsunematsu Y, Kikuta A, Kaneko Y (2007) Promoter hypermethylation of the *RASSF1A* gene predicts the poor outcome of patients with hepatoblastoma. *Pediatr Blood Cancer* **49:** 240–249

Suzuki M, Kato M, Yuyan C, Takita J, Sanada M, Nannya Y, Yamamoto G, Takahashi A, Ikeda H, Kuwano H, Ogawa S, Hayashi Y (2008) Whole-genome profiling of chromosomal aberrations in hepatoblastoma using high-density single-nucleotide polymorphism genotyping microarrays. *Cancer Sci* **99:** 564–570

Takai D, Gonzales FA, Tsai YC, Thayer MJ, Jones PA (2001) Large scale mapping of methylcytosines in CTCF-binding sites in the human *H19* promoter and aberrant hypomethylation in human bladder cancer. *Hum Mol Genet* **10:** 2619–2626

Taniguchi K, Roberts LR, Aderca IN, Dong X, Qian C, Murphy LM, Nagorney DM, Burgart LJ, Roche PC, Smith DI, Ross JA, Liu W (2002) Mutational spectrum of beta-catenin, *AXIN1*, and *AXIN2* in hepatocellular carcinomas and hepatoblastomas. *Oncogene* **21:** 4863–4871

Toretsky JA, Helman LJ (1996) Involvement of IGF-II in human cancer. *J Endocrinol* **149:** 367–372

Vu TH, Hoffman AR (1999) Alterations in the promoter-specific imprinting of insulin-like growth factor-II gene in Wilms tumor. *J Biol Chem* **271:** 9014–9023

Wang WH, Duan JX, Vu TH, Hoffman AR (1996) Increased expression of the insulin-like growth factor-II gene in Wilms' tumor is not dependent on loss of genomic imprinting or loss of heterozygosity. *J Biol Chem* **271:** 27863–27870

Watanabe N, Haruta M, Soejima H, Fukushi D, Yokomori K, Nakadate H, Okita H, Hata J, Fukuzawa M, Kaneko Y (2007) Duplication of the paternal *IGF2* allele in trisomy 11 and elevated expression levels of *IGF2* mRNA in congenital mesoblastic nephroma of the cellular or mixed type. *Genes Chromosomes Cancer* **46:** 929–935

Watanabe N, Nakadate H, Haruta M, Sugawara W, Sasaki F, Tsunematsu Y, Kikuta A, Fukuzawa M, Okita H, Hata J, Soejima H, Kaneko Y (2006) Association of 11q loss, trisomy 12, and possible 16q loss with loss of imprinting of insulin-like growth factor-II in Wilms tumor. *Genes Chromosomes Cancer* **45:** 592–601

Yuan E, Li CM, Yamashiro DJ, Kandel J, Thaker H, Murty VV, Tycko B (2005) Genomic profiling maps loss of heterozygosity and defines the timing and stage dependence of epigenetic and genetic events in Wilms' tumors. *Mol Cancer Res* **3:** 493–502

Zatkova A, Rouillard JM, Hartmann W, Lamb BJ, Kuick R, Eckart M, von Schweinitz D, Koch A, Fonatsch C, Pietsch T, Hanash SM, Wimmer K (2004) Amplification and overexpression of the *IGF2* regulator *PLAG1* in hepatoblastoma. *Genes Chromosomes Cancer* **39:** 126–137

MOLECULAR CARCINOGENESIS 47:660–666 (2008)

BRIEF COMMUNICATION

Combined BubR1 Protein Down-Regulation and *RASSF1A* Hypermethylation in Wilms Tumors With Diverse Cytogenetic Changes

Masayuki Haruta,[1]* Yoshiyuki Matsumoto,[2] Hideki Izumi,[2] Naoki Watanabe,[1] Masahiro Fukuzawa,[3] Shinya Matsuura,[2] and Yasuhiko Kaneko[1,3]

[1]*Research Institute for Clinical Oncology, Saitama Cancer Center, Ina, Saitama, Japan*
[2]*Research Institute for Radiation Biology and Medicine, Hiroshima University, Hiroshima, Hiroshima, Japan*
[3]*Japan Wilms Tumor Study Group, Itabashi-Ku, Tokyo, Japan*

BUB1B and *RASSF1A* genes play specific roles in the mitotic checkpoint, and their defects may cause chromosome instability or aneuploidy in mouse fibroblasts and human cancer cell lines; however, few studies have reported a correlation between defects in these genes and chromosome changes in human tumor samples. We examined chromosome abnormalities in 25 Wilms tumors by metaphase comparative genomic hybridization, and classified them into 14 hyperdiploid (50 ≥ chromosomes), 2 near-or-pseudodiploid, and 9 diploid tumors. We also examined various molecular aspects of *BUB1B* and *RASSF1A*, and evaluated the relationship between chromosome changes and the status of both genes. No tumors showed *BUB1B* mutation. BubR1 protein (*BUB1B* gene product) expression was undetectable or decreased in five of six hyperdiploid or near-or-pseudodiploid tumors and increased in four of five diploid tumors, whereas all seven tumors examined showed *BUB1B* mRNA expression irrespective of their chromosome pattern. Furthermore, while complete promoter methylation of *RASSF1A* was found in 13 of 16 hyperdiploid or near-or-pseudodiploid tumors, unmethylated *RASSF1A* was found in 5 of 9 diploid tumors. Partial *RASSF1A* methylation was found in three hyperdiploid or near-or-pseudodiploid tumors and in four diploid tumors. Thus, BubR1 protein expression decreased, and the promoter region of *RASSF1A* was completely methylated in the great majority of hyperdiploid or near-or-pseudodiploid tumors, BubR1 protein expression increased and *RASSF1A* was unmethylated in the majority of diploid tumors. These findings suggest that the combined BubR1 protein down-regulation and *RASSF1A* hypermethylation might be implicated in the formation of chromosomal changes found in Wilms tumors.

Key words: Wilms tumor; *BUB1B*; BubR1 protein expression; *RASSF1A* hypermethylation; chromosome changes

INTRODUCTION

Aneuploidy is a hallmark of cancer, and defects in mitotic checkpoint genes may cause aneuploidy and might promote tumorigenesis [1]. Mouse fibroblasts with reduced levels of Mad1, Mad2, Bub1b, or Bub3 have shown chromosomal instability, and significant increases in the number of aneuploid cells [2–5]. *RASSF1A*, whose promoter methylation is frequently found in various cancers, including Wilms tumor, regulates the stability of mitotic cyclins and the timing of mitotic progression, and its defect caused centrosome abnormalities and multipolar spindles in human cancer cell lines [6–9].

Recently, homozygous and heterozygous mutations of *BUB1B* were found in mosaic variegated aneuploidy (MVA) and premature chromatid separation (PCS) syndromes, respectively, which were clinically characterized by severe intrauterine growth retardation, microcephaly, and eye anomalies [10–12]. Patients with each syndrome are prone to develop Wilms tumor and rhabdomyosarcoma. Karyotypes of two Wilms tumors occurring in patients with PCS syndrome were reported, and showed hyperdiploidy with nonrandom extra chromosomes [13]. We have previously proposed that hyperdiploid Wilms tumors with 50 or more chromosomes may be a genetic subgroup of Wilms tumor characterized by

Abbreviations: PCS, premature chromatid separation; mCGH, metaphase comparative genomic hybridization; RT, reverse-transcription; MSP, methylation-specific PCR; SNP, single-nucleotide polymorphism.

*Correspondence to: Research Institute for Clinical Oncology, Saitama Cancer Center, Komuro 818, Ina, Kitaadachi-gun, Saitama 362-0806, Japan.

Received 11 March 2007; Revised 16 November 2007; Accepted 20 November 2007

DOI 10.1002/mc.20412

Published online 19 February 2008 in Wiley InterScience (www.interscience.wiley.com)

nonrandom extra chromosomes and the absence of *WT1* deletions/mutations [14].

As hyperdiploid Wilms tumor developed in patients with PCS syndrome, we speculated that *BUB1B* mutation might be involved in the neoplastic process of sporadic hyperdiploid Wilms tumor. In addition, although the reduced expression of mitotic checkpoint genes caused chromosomal aneuploidy in mice [2–5], few studies have reported the relationship between chromosomal changes and genetic and epigenetic alterations of the mitotic checkpoint genes in human cancer samples. Thus, we examined mutations and protein expression levels of the *BUB1B* gene and the methylation status of the promoter region of *RASSF1A* in diploid, near-or-pseudodiploid and hyperdiploid Wilms tumors. While undetectable or decreased protein expression levels of BubR1 and complete promoter methylation of *RASSF1A* were found in the great majority of hyperdiploid or near-or-pseudodiploid tumors, increased protein expression levels of BubR1 and unmethylation of *RASSF1A* were found in the majority of diploid tumors. These findings suggest that down-regulation of the BubR1 protein expression and promoter hypermethylation of *RASSF1A* might be related to the chromosome changes found in the majority of Wilms tumors.

MATERIALS AND METHODS

Patient Samples

Tumor samples were obtained from 25 Japanese infants or children ranging in age from 2 months to 15 yr who underwent surgery or biopsy between August 1984 and February 2003. Patients were selected based on the availability of tumor DNA, RNA, and protein. All 25 tumors were diagnosed as Wilms tumor of favorable histology [15]. One patient (No. 17) had Wilms tumor associated with aniridia, and/or genitourinary malformation (WAGR syndrome), and the remaining 24 patients had a sporadic unilateral tumor. Two normal kidney tissue samples adjacent to a Wilms tumor were obtained from 2 patients whose tumor samples were not included in the 25 tumors described above.

Metaphase Comparative Genomic Hybridization (mCGH) Studies

mCGH analysis was performed also as described previously [16]. A chromosomal region was considered to be overrepresented or underrepresented if the average ratio profile was above 1.25 or below 0.75, respectively.

Mutation Analyses of *WT1* and *BUB1B*

Mutational analysis of *WT1* was performed as described previously [14]. PCR primers used for *BUB1B* mutational analysis were designed to amplify all coding exons of *BUB1B* and at least 50 bp of the intronic sequences that contained 5′ and 3′ splice junctions [12]. PCR products were directly sequenced on a sequencer (Applied Biosystems, Foster City, CA).

Western Blot Analysis of BubR1

Western blot analysis using rabbit anti-BubR1 polyclonal antibody raised against human BubR1 (amino acids 1–478) was performed as described previously [12]. α-tubulin detected by mouse anti α-tubulin monoclonal antibody (Sigma–Aldrich, St. Louis, MO) was used as a control for protein loading. Protein extracted from human immortalized skin fibroblast cells was used as a positive control of BubR1. The experiment was performed at least twice, and the results are summarized in Table 1 and Figure 1.

Reverse-Transcription (RT)-PCR Analysis of *BUB1B*

First strand cDNA synthesis was carried out with PrimeScript™ 1st strand cDNA synthesis kit (TAKARA, Ohtsu, Japan) according to the manufacturer's protocol. The PCR was performed with AmpliTaq Gold (Applied Biosystems). PCR primers used were reported previously [17]. PCR products were analyzed by electrophoresis in a 2.0% agarose gel and stained with ethidium bromide (Sigma–Aldrich).

Methylation-Specific PCR (MSP), Bisulfite DNA Sequencing and Quantitative Methylation Analysis of the *RASSF1A* Promoter Region

Genomic DNA from tumor and normal kidney samples was treated with sodium bisulfite as previously described [18]. Bisulfite-modified DNA was amplified as previously described with primers specific for methylated and unmethylated sequences of *RASSF1A* gene promoter regions [18]. Normal lymphocyte DNA treated or untreated with *Sss*I methyltransferase (New England Biolabs, Ipswich, MA) was used as a control for methylated or unmethylated templates, respectively. The amplification primers used for bisulfite DNA sequencing were previously reported. PCR products were inserted into the vectors, and 10 clones from each tumor DNA were sequenced.

Quantitative methylation analysis was performed using LightCycler TaqMan Master on the Light-Cycler Carousel-Based System (Roche Diagnostics, Alameda, CA) according to the manufacturer's protocol. The actin beta gene (*ACTB*) was used as an internal reference to control for input DNA. The primers and probes used for *RASSF1A* and *ACTB* quantification, and PCR conditions were previously reported [19,20]. Differences in the average quantity of methylated templates between tumors with complete *RASSF1A* methylation and those with partial *RASSF1A* methylation were examined by Student's *t*-test and Welch's *t*-test.

Table 1. BubR1 Protein and *BUB1B* mRNA Expression and Methylation and mRNA Expression Status of *RASS1A* in Wilms Tumors Classified by Metaphase CGH Pattern

Tumor number	Metaphase CGH pattern	BubR1 protein expression	*BUB1B* mRNA	*RASSF1A*		
				MSP	Quantification	mRNA
Hyperdiploid tumors (≥50 chromosomes) ($n = 14$)						
1	enh(1q, 2, 4, 6, 12), dim(1p13-1pter, 3p, 11, 13q14-qter)	+	ND	M	0.34	ND
2	enh(1q, 2, 6, 7q21-qter, 8, 10, 12pter-q23, 13, 15), dim(1p, 18p)	±	ND	M	0.42	ND
3	enh(1q, 7, 10, 12, 13), dim(11q22-qter)	−	+	M	0.32	−
4	enh(1q, 2, 7, 12, 20)	−	+	M	0.36	−
5	enh(1q, 6, 8, 9, 10, 12, 17, 18)	±	ND	M	0.72	ND
6–11	Various changes	ND	ND	M	0.62, 0.65, 0.66, 0.37, 0.65, 0.85	ND
12–14	Various changes	ND	ND	M + U	0.22, 0.40, 0.30	ND
Near-or-pseudodiploid tumors ($n = 2$)						
15	enh(7q),dim(7p)	−	+	M	0.60	±
16	enh(12),dim(9, 10p, 11q, 16q, 18p)	ND	ND	M	0.64	ND
Diploid tumors ($n = 9$)						
17[a]	Normal	++	ND	M + U	0.34	ND
18	Normal	++	ND	U	0	ND
19	Normal	++	ND	M + U	0.23	ND
20[b]	Normal	++	+	M + U	0.29	−
21	Normal	+	+	M + U	0.39	−
22, 22	Normal	ND	ND	U	0, 0	ND
24, 25	Normal	ND	+	U	0, 0	+
Two normal kidney tissues		−	−	U	0, 0	+
Fetal kidney tissues		ND	−	ND	ND	ND
Human immortalized skin fibroblast cells		++	+	ND	ND	ND

ND, not done; M, methylated band only; M + U, methylated and unmethylated bands; U, unmethylated band only.
[a]The tumor that occurred in a WAGR patient had a hemizygous deletion and a point mutation in exon 8 of *WT1*.
[b]The tumor that occurred in a sporadic patient had a hemizygous deletion and a point mutation in exon 10 of *WT1*.

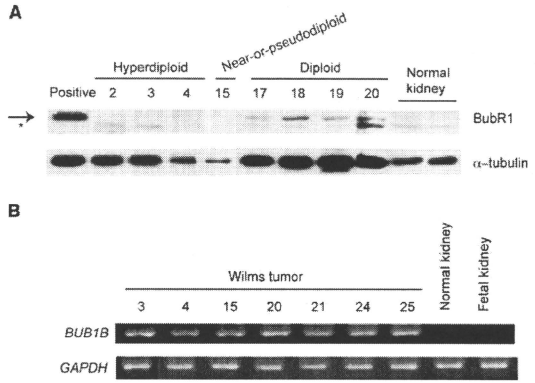

Figure 1. Examples of BubR1 protein and *BUB1B* mRNA expression in Wilms tumors. (A) Western blot showed BubR1 protein and non-specific staining, indicated by an arrow and asterisk, respectively. (B) RT-PCR showed *BUB1B* mRNA expression in all Wilms tumor tissues with various karyotypes, but not in a normal kidney tissue and fetal kidney RNA.

RT-PCR Analysis of *RASSF1A*

RT-PCR analysis of *RASSF1A* was performed as previously described [18].

RESULTS AND DISCUSSION

In mCGH analysis of 25 Wilms tumors, 14 had hyperdiploidy (≥50 chromosomes), 2 had near-or-pseudodiploidy, and 9 had normal diploidy (Table 1). In subsequent sequence analysis of whole exons of the *BUB1B* gene, no mutation was found in all 25 tumors. We found a single-nucleotide polymorphism (SNP), 1064G/A or G > A (rs1601375) at exon 8 of *BUB1B* in 15, and another SNP, 1164G/A or G > A at exon 9 in 4 of the 25 tumors. Four tumors showed heterozygosity only at the SNP site in exon 8, 2 tumors only at the SNP site in exon 9, and one tumor at both sites. Thus, seven tumors retained heterozygosity at the *BUB1B* locus. mCGH analysis showed that the remaining 16 tumors with homozygosity at the locus showed no loss of chromosome 15, supporting that no hemizygous deletion occurred at the locus. Karyotypes of 2 Wilms tumors in patients with PCS syndrome were reported, and showed hyperdiploidy with 48–55 chromosomes, including extra chromosomes 6, 8, 12, 13, 15, 17, and 18 [13]. These karyotypes were similar to those found in hyperdiploid Wilms tumors developed in sporadic patients [14]. Therefore, we speculated that hyperdiploid Wilms tumors of sporadic origin might have *BUB1B* mutations; however, no mutation of the gene was found in either hyperdiploid or non-hyperdiploid tumors. Hanks et al. [21] recently reported no mutation of *BUB1B* in 30 sporadic Wilms tumors although they did not show cytogenetic data, and the present findings were consistent with theirs.

Epigenetic silencing of cancer-related genes is an important mechanism for the development and progression of cancer [22], and one study reported epigenetic down-regulation of *BUB1B* mRNA in some colorectal cancers [23]. In the present study, we examined protein expression levels of BubR1 in 11 Wilms tumors with Western blotting, and showed undetectable or decreased protein expression levels of BubR1 in 5 of 6 hyperdiploid or near-or-pseudodiploid tumors, increased expression levels in 4 of 5 diploid tumors and human immortalized skin fibroblast cells, and undetectable expression levels in two control normal kidney tissues (Table 1 and Figure 1A). Contrary to these findings, *BUB1B* mRNA, which was undetectable in normal and fetal kidney (Clontech, Ohtsu, Japan) tissues, was expressed in all Wilms tumors irrespective of their chromosome pattern (Table 1 and Figure 1B). These findings indicate that BubR1 and *BUB1B* mRNA may be expressed in diploid Wilms tumors, as previously reported in most breast cancer tissues, probably because of the predominance of proliferating cells [17,24]. In contrast, *BUB1B* mRNA may be expressed, but BubR1 may be down-regulated subsequent to the neoplastic transformation of hyperdiploid or near-or-pseudodiploid

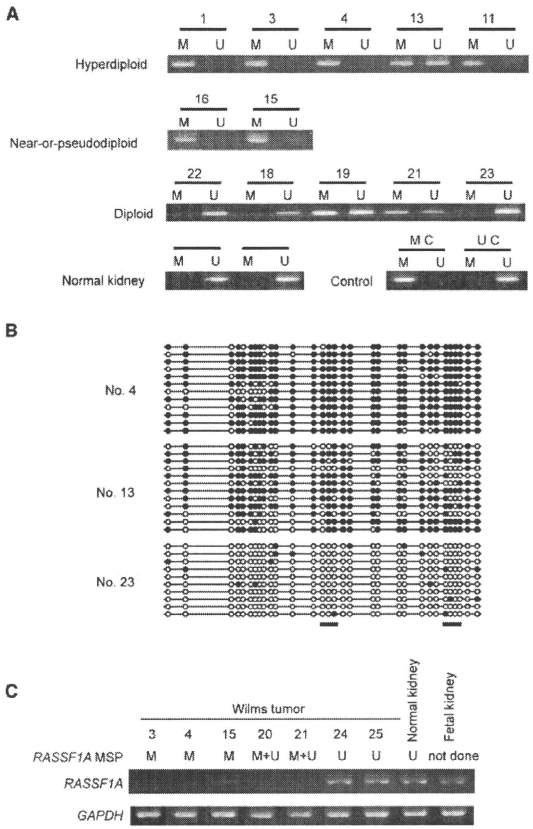

Figure 2. Methylation status of the *RASSF1A* promoter region and *RASSF1A* mRNA expression in Wilms tumors. (A) Examples of promoter methylation status using methylation-specific PCR. M, methylated promoter; U, unmethylated promoter; MC, a methylated control using methylated DNA; UC, an unmethylated control using unmethylated DNA. (B) Bisulfite sequencing analysis of the methylation status of *RASSF1A* in three Wilms tumors (Nos. 4, 13, and 23) shown in (A). The locations of MSP primers are shown at the bottom of the figure. (C) *RASSF1A* mRNA expression analysis by RT-PCR.

Wilms tumors. The mechanism causing the down-regulation of BubR1 is presently unknown, and may include the suppressed translation by miRNA, the accelerated ubiquitination that degrades protein [25,26], et cetera, but not by methylation of the promoter region.

BubR1 is a key molecule mediating spindle-checkpoint activation. Recent mouse studies showed

that haplo-insufficiency of *BubR1* results in enhanced genomic instability and cancer development in the lung and colon, leading to a speculation that haplo-insufficiency of *BubR1* can cause genetic instabilities at the levels of both DNA repair and chromosomal segregation, the deregulation of which will inevitably result in malignant transformation [4,27,28]. Structural chromosomal changes, including translocations and deletions, are thought to occur through DNA double-strand break repair after DNA damage [29]. Thus, these findings and ours indicated that the down-regulation of *BUB1B* might be involved in the occurrence of sporadic hyperdiploid and near-or-pseudodiploid Wilms tumors.

RASSF1A is a candidate tumor suppressor gene that has been shown to play important roles in cell cycle regulation, apoptosis, and microtubule stability [6]. RASSF1A protein associates with microtubules in interphase, and spindles and centrosomes during mitosis, and blocks activated Ras-induced genomic instability [30,31]. In addition, Song et al. [7] identified *RASSF1A* as a mitosis-specific inhibitor of anaphase-promoting complex/cyclosome (APC/C). They also showed that depletion of the gene by RNA interference accelerated mitotic cyclin degradation and mitotic progression, and caused a cell division defect characterized by centrosome abnormalities and multipolar spindles. Thus, loss of *RASSF1A* expression might be involved in chromosome abnormalities. Methylation of the *RASSF1A* promoter was frequently reported in various cancers, including Wilms tumor [6,8,9], and previous studies repeatedly showed that promoter hypermethylation of *RASSF1A* correlated with loss of expression and treatment with a demethylating agent reactivated *RASSF1A* gene expression in various cancer tissues or cell lines [32–34]. There have been few reports that examined the relationship between *RASSF1A* methylation and chromosome changes in tumor samples. We therefore analyzed the methylation status of the *RASSF1A* promoter region in 25 Wilms tumors with MSP and found complete methylation in 13 of 16 hyperdiploid or near-or-pseudodiploid tumors, and unmethylation of *RASSF1A* in 5 of 9 diploid tumors (Table 1 and Figure 2A). The partial promoter methylation was found in 3 hyperdiploid or near-or-pseudodiploid tumors and in 4 diploid tumors. The results of MSP analysis were confirmed by bisulfite sequencing and quantitative methylation analysis that showed higher levels of methylated *RASSF1A* templates in tumors with the compete methylation than in tumors with the unmethylation or partial methylation ($P < 0.01$; Student's *t*-test and Welch's *t*-test) (Figure 2B and Table 1). Furthermore, RT-PCR analysis detected *RASSF1A* mRNA in diploid Wilms tumors and normal kidney tissues with unmethylated *RASSF1A*, but essentially not in hyperdiploid or near-or-pseudodiploid tumors with completely or partially methylated *RASSF1A* (Table 1 and Figure 2C); one tumor (No. 15) with the complete methylation showed a faint band probably because of contaminated normal tissue RNA. Chromosome instability was found in Hela cells treated with *RASSF1A* RNA interference, but not in *Rassf1a* knockout mice [7,30]. These findings led us to speculate that the combined down-regulation of *RASSF1A* and other genes may cause chromosome instability in tumor cells.

Thus, while BubR1 protein expression decreased and the promoter region of *RASSF1A* was completely methylated in the great majority of hyperdiploid or near-or-pseudodiploid tumors, BubR1 protein expression increased and the promoter region of *RASSF1A* was unmethylated in the majority of diploid tumors. Partial methylation of *RASSF1A* was found in both groups of tumors with or without chromosome changes, and its significance on the changes is unresolved in the present study. There was no correlation between histological subtypes of Wilms tumor and decreased BubR1 protein expression or *RASSF1A* hypermethylation (data not shown). These findings indicate that the combined down-regulation of BubR1 and promoter hypermethylation of *RASSF1A* might be implicated in the formation of numerical and/or structural chromosomal changes found in hyperdiploid and near-or-pseudodiploid Wilms tumors.

ACKNOWLEDGMENTS

The authors thank the physicians and parents who participated in the Japan Wilms tumor study group and supplied samples for this study. This work was supported by Grants-in-Aid from the Ministry of Health, Labor, and Welfare, Japan for the 3rd-term Comprehensive 10-yr Strategy for Cancer Control and from the Ministry of Education, Science, Sports and Culture of Japan (18790745), and Kawano Masanori Memorial Foundation for the Promotion of Pediatrics.

REFERENCES

1. Kops GJ, Weaver BA, Cleveland DW. On the road to cancer: Aneuploidy and the mitotic checkpoint. Nat Rev Cancer 2005;5:773–785.
2. Michel LS, Liberal V, Chatterjee A, et al. *MAD2* haplo-insufficiency causes premature anaphase and chromosome instability in mammalian cells. Nature 2001;409:355–359.
3. Babu JR, Jeganathan KB, Baker DJ, Wu X, Kang-Decker N, van Deursen JM. Rae1 is an essential mitotic checkpoint regulator that cooperates with Bub3 to prevent chromosome missegregation. J Cell Biol 2003;160:341–353.
4. Dai W, Wang Q, Liu T, et al. Slippage of mitotic arrest and enhanced tumor development in mice with *BubR1* haploinsufficiency. Cancer Res 2004;64:440–445.
5. Iwanaga Y, Chi YH, Miyazato A, et al. Heterozygous deletion of mitotic arrest-deficient protein 1 (MAD1) increases the incidence of tumors in mice. Cancer Res 2007;67:160–166.

6. Agathanggelou A, Cooper WN, Latif F. Role of the Ras-association domain family 1 tumor suppressor gene in human cancers. Cancer Res 2005;65:3497–3508.
7. Song MS, Song SJ, Ayad NG, et al. The tumour suppressor RASSF1A regulates mitosis by inhibiting the APC-Cdc20 complex. Nat Cell Biol 2004;6:129–137.
8. Ehrlich M, Jiang G, Fiala E, et al. Hypomethylation and hypermethylation of DNA in Wilms tumors. Oncogene 2002; 21:6694–6702.
9. Wagner KJ, Cooper WN, Grundy RG, et al. Frequent RASSF1A tumour suppressor gene promoter methylation in Wilms' tumour and colorectal cancer. Oncogene 2002;21: 7277–7282.
10. Kajii T, Ikeuchi T, Yang ZQ, et al. Cancer-prone syndrome of mosaic variegated aneuploidy and total premature chromatid separation: Report of five infants. Am J Med Genet 2001; 104:57–64.
11. Hanks S, Coleman K, Reid S, et al. Constitutional aneuploidy and cancer predisposition caused by biallelic mutations in *BUB1B*. Nat Genet 2004;36:1159–1161.
12. Matsuura S, Matsumoto Y, Morishima K, et al. Monoallelic *BUB1B* mutations and defective mitotic-spindle checkpoint in seven families with premature chromatid separation (PCS) syndrome. Am J Med Genet A 2006;140:358–367.
13. Ikeuchi T, Yoshida M, Oda S, et al. Cytogenetic changes in tumor cells of patients with premature chromatid separation (PCS) syndrome, presented at 49th annual meeting of the Japan society of human genetics, Tokyo, Japan: In abstract; 2004. p 126.
14. Nakadate H, Tsuchiya T, Maseki N, et al. Correlation of chromosome abnormalities with presence or absence of *WT1* deletions/mutations in Wilms tumor. Genes Chromosomes Cancer 1999;25:26–232.
15. Beckwith JB, Palmer NF. Histopathology and prognosis of Wilms tumors: Results from the First National Wilms' Tumor Study. Cancer 1978;41:1937–1948.
16. Kumon K, Kobayashi H, Namiki T, et al. Frequent increase of DNA copy number in the 2q24 chromosomal region and its association with a poor clinical outcome in hepatoblastoma: Cytogenetic and comparative genomic hybridization analysis. Jpn J Cancer Res 2001;92:854–862.
17. Yuan B, Xu Y, Woo JH, et al. Increased expression of mitotic checkpoint genes in breast cancer cells with chromosomal instability. Clin Cancer Res 2006;12:405–410.
18. Sugawara W, Haruta M, Watanabe N, Tsunematsu Y, Kikuta A, Kaneko Y. Promoter hypermethylation of the *RASSF1A* gene predicts the poor outcome of patients with hepatoblastoma. Pediatr Blood Cancer 2007;49:240–249.
19. Schmiemann V, Bocking A, Kazimirek M, et al. Methylation assay for the diagnosis of lung cancer on bronchial aspirates: A cohort study. Clin Cancer Res 2005;11:7728–7734.
20. Hoque MO, Begum S, Topaloglu O, et al. Quantitation of promoter methylation of multiple genes in urine DNA and bladder cancer detection. J Natl Cancer Inst 2006;98:996–1004.
21. Hanks S, Coleman K, Summersgill B, et al. Comparative genomic hybridization and *BUB1B* mutation analyses in childhood cancers associated with mosaic variegated aneuploidy syndrome. Cancer Lett 2006;239:234–238.
22. Baylin SB, Ohm JE. Epigenetic gene silencing in cancer—A mechanism for early oncogenic pathway addiction? Nat Rev Cancer 2006;2:107–116.
23. Shichiri M, Yoshinaga K, Hisatomi H, Sugihara K, Hirata Y. Genetic and epigenetic inactivation of mitotic checkpoint genes *hBUB1* and *hBUBR1* and their relationship to survival. Cancer Res 2002;62:13–17.
24. Davenport JW, Fernandes ER, Harris LD, Neale GA, Goorha R. The mouse mitotic checkpoin gne bub1b, a novel bub1 family member, is expressed in a cell cycle-dependent manner. Genomics 1999;55:113–117.
25. Bartel DP. MicroRNAs: Genomics, biogenesis, mechanism, and function. Cell 2004;116:281–297.
26. King EMJ, van der Sar SJ, Hardwick KG. Mad3 KEN boxes mediate both Cdc20 and Mad3 turnover, and are critical for the spindle checkpoint. PLoS ONE 2007;4:e342 (1–12).
27. Rao CV, Yang YM, Swamy MV, et al. Colonic tumorigenesis in *BubR1+/-ApcMin+/-* compound mutant mice is linked to premature separation of sister chromatids and enhanced genomic instability. Proc Natl Acad Sci USA 2005;102:4365–4370.
28. Fang Y, Liu T, Wang X, et al. BubR1 is involved in regulation of DNA damage responses. Oncogene 2006;25:3598–3605.
29. Ferguson DO, Alt FW. DNA double strand break repair and chromosomal translocation: Lessons from animal models. Oncogene 2001;20:5572–5579.
30. Liu L, Tommasi S, Lee DH, Dammann R, Pfeifer GP. Control of microtubule stability by the RASSF1A tumor suppressor. Oncogene 2003;22:8125–8136.
31. Vos MD, Martinez A, Elam C, et al. A role for the RASSF1A tumor suppressor in the regulation of tubulin polymerization and genomic stability. Cancer Res 2004;64:4244–4250.
32. Hesson L, Bieche I, Krex D, et al. Frequent epigenetic inactivation of *RASSF1A* and *BLU* genes located within the critical 3p21.3 region in gliomas. Oncogene 2004;23:2408–2419.
33. Harada K, Toyooka S, Maitra A, et al. Aberrant promoter methylation and silencing of the *RASSF1A* gene in pediatric tumors and cell lines. Oncogene 2002;21:4345–4349.
34. Dammann R, Li C, Yoon JH, Chin PL, Bates S, Pfeifer GP. Epigenetic inactivation of a RAS association domain family protein from the lung tumour suppressor locus 3p21.3. Nat Genet 2000;25:315–319.

MOLECULAR AND CELLULAR BIOLOGY, Apr. 2008, p. 2125–2137 Vol. 28, No. 7
0270-7306/08/$08.00+0 doi:10.1128/MCB.00740-07

Inducible Expression of Chimeric EWS/ETS Proteins Confers Ewing's Family Tumor-Like Phenotypes to Human Mesenchymal Progenitor Cells▽†

Yoshitaka Miyagawa,[1] Hajime Okita,[1]* Hideki Nakaijima,[1] Yasuomi Horiuchi,[1] Ban Sato,[1] Tomoko Taguchi,[1] Masashi Toyoda,[3] Yohko U. Katagiri,[1] Junichiro Fujimoto,[2] Jun-ichi Hata,[1] Akihiro Umezawa,[3] and Nobutaka Kiyokawa[1]

Department of Developmental Biology, National Research Institute for Child Health and Development, 2-10-1, Okura, Setagaya-ku, Tokyo 157-8535, Japan[1]; National Research Institute for Child Health and Development, 2-10-1, Okura, Setagaya-ku, Tokyo 157-8535, Japan[2]; and Department of Reproductive Biology, National Research Institute for Child Health and Development, 2-10-1, Okura, Setagaya-ku, Tokyo 157-8535, Japan[3]

Received 27 April 2007/Returned for modification 13 July 2007/Accepted 7 January 2008

Ewing's family tumor (EFT) is a rare pediatric tumor of unclear origin that occurs in bone and soft tissue. Specific chromosomal translocations found in EFT cause EWS to fuse to a subset of ets transcription factor genes (ETS), generating chimeric EWS/ETS proteins. These proteins are believed to play a crucial role in the onset and progression of EFT. However, the mechanisms responsible for the EWS/ETS-mediated onset remain unclear. Here we report the establishment of a tetracycline-controlled EWS/ETS-inducible system in human bone marrow-derived mesenchymal progenitor cells (MPCs). Ectopic expression of both EWS/FLI1 and EWS/ERG proteins resulted in a dramatic change of morphology, i.e., from a mesenchymal spindle shape to a small round-to-polygonal cell, one of the characteristics of EFT. EWS/ETS also induced immunophenotypic changes in MPCs, including the disappearance of the mesenchyme-positive markers CD10 and CD13 and the up-regulation of the EFT-positive markers CD54, CD99, CD117, and CD271. Furthermore, a prominent shift from the gene expression profile of MPCs to that of EFT was observed in the presence of EWS/ETS. Together with the observation that EWS/ETS enhances the ability of cells to invade Matrigel, these results suggest that EWS/ETS proteins contribute to alterations of cellular features and confer an EFT-like phenotype to human MPCs.

Ewing's family tumor (EFT) is a rare childhood cancer arising mainly in bone and soft tissue. Since EFT has a poor prognosis, it is important to elucidate the underlying pathogenic mechanisms for establishing a more effective therapeutic strategy. EFT is characterized by the presence of chimeric genes composed of EWS and ets transcription factor genes (ETS) formed by specific chromosomal translocations, i.e., EWS/FLI1, t(11;22)(q24;q12); EWS/ERG, t(21;22)(q12;q12); EWS/ETV1, t(7;22)(p22;q12); EWS/E1AF, t(17;22)(q12;q12); and EWS/FEV, t(2;22)(q33;q12) (26). The products of these chimeric genes behave as aberrant transcriptional regulators and are believed to play a crucial role in the onset and progression of EFT (3, 36). Indeed, recent studies have revealed that the induction of EWS/FLI1 proteins can trigger transformation in certain cell types, including NIH 3T3 cells (36), C2C12 myoblasts (12), and murine primary bone marrow-derived mesenchymal progenitor cells (MPCs) (6, 45, 52). However, studies have also indicated that overexpression of EWS/FLI1 provokes apoptosis and growth arrest in mouse normal embryonic fibroblasts and primary human fibroblasts (10, 31), hence hampering understanding of the precise role of EWS/ETS proteins in the development of EFT. The function of EWS/ETS proteins would be greatly influenced by cell type, and thus the cells that can originate EFTs might be more susceptible to the tumorigenic effects of EWS/ETS.

Although the cell origin of EFT is still unknown, the expression of neuronal markers in spite of the occurrence in bone and soft tissues has kept open the debate as to a potential mesenchymal or neuroectodermal origin. As described above, ectopic expression of EWS/FLI1 results in dramatic changes in morphology and the formation of EFT-like tumors in murine primary bone marrow-derived MPCs but not in murine embryonic stem cells (6, 45, 52), supporting the notion that MPCs are a plausible cell origin of EFT (45). However, others argue that MPCs cannot be considered progenitors of EFT without further evidence of similarity between human EFT and MPC-EWS/FLI1-induced tumors in mice (29, 46).

The development of experimental systems using murine species is useful for elucidating the mechanisms behind the pathogenesis of EFT. However, several differences between human and murine systems cannot be ignored; these differences include the expression patterns of surface antigens in MPCs, for instance (7, 44, 51, 53). Moreover, human cells are difficult to transform in vitro, and the transformed cells of mice seem to produce a more aggressive tumor than those of hu-

* Corresponding author. Mailing address: Department of Developmental Biology, National Research Institute for Child Health and Development, 2-10-1, Okura, Setagaya-ku, Tokyo 157-8535, Japan. Phone: 81-3-3416-0181. Fax: 81-3-3417-2496. E-mail: okita@nch.go.jp.

† Supplemental material for this article may be found at http://mcb.asm.org/.

▽ Published ahead of print on 22 January 2008.

TABLE 1. Cell lines used in this study and fusion transcript types

Cell line	Diagnosis	Fusion transcript type	Reference
EES-1	EFT	EWS/FLI1 type I	20
SCCH196	EFT	EWS/FLI1 type I	21
RD-ES	EFT	EWS/FLI1 type II	5
SK-ES1	EFT	EWS/FLI1 type II	5
NCR-EW2	EFT	EWS/FLI1 type II	19
NCR-EW3	EFT	EWS/E1AF	19
W-ES	EFT	EWS/ERG	13
NB69	NB		15
NB9	NB		15
GOTO	NB		47
NRS-1	RMS	PAX3/FKHR	40

mans (1). The findings suggest the existence of undefined cell-autonomous mechanisms that render human cells resistant to malignant transformation. Therefore, the use of human cell models is ideal for clarifying how EFT develops. Models of the onset of EFT have been generated using primary fibroblasts (31) and rhabdomyosarcoma cells (23). However, these cell types are not appropriate for studying the origins of EFT, and a model that precisely recapitulates EWS/ETS-mediated EFT formation is required.

UET-13 cells are obtained by prolonging the life span of human bone marrow stromal cells by use of the retroviral transgenes hTERT and E7 (38, 50), retain the ability to differentiate into not only mesodermal derivatives but also neuronal progenitor-like cells, and are considered a good model for studying the cellular events in human MPCs. Therefore, we have examined the biological effect of EWS/ETS in human MPCs by use of UET-13 cells by exploiting tetracycline-inducible systems for expressing EWS/ETS (EWS/FLI1 and EWS/ERG). Here we report that overexpression of EWS/ETS mediates an EFT-like phenotype, including morphology, immunophenotype, and gene expression profile, with enhancement of the Matrigel invasion ability of UET-13 cells.

MATERIALS AND METHODS

Cell cultures and establishment of UET-13TR-EWS/ETS cell lines. UET-13 cells were cultured in Dulbecco's modified Eagle's medium (DMEM) with 10% Tet system approved fetal bovine serum (T-FBS) (Takara) at 37°C under a humidified 5% CO_2 atmosphere. EFT cell lines (EES-1 [20], SCCH196 [21], RD-ES and SK-ES1 [5], NCR-EW2 and NCR-EW3 [19], and W-ES [13]) and neuroblastoma (NB) cell lines (NB69 and NB9 [15] and GOTO [47]) were cultured in RPMI 1640 with 10% FBS. A rhabdomyosarcoma cell line, NRS-1 (40), was cultured in Eagle's minimal essential medium with 10% FBS. The cell lines used in this study are listed in Table 1.

UET-13 cells were seeded at a density of 5×10^4 cells per well in 24-well tissue culture plates 1 day prior to transfection. For introducing the tetracycline-inducible system, UET-13 cells were transfected with pcDNA6-TR (Invitrogen) by use of Lipofectamine 2000 (Invitrogen). After 72 h, the medium was replaced with fresh medium containing 200 μg/ml of blasticidin S (Invitrogen). Individual resistant clones were selected for a month and designated UET-13TR cells. UET-13TR cells were further transfected with pcDNA4-EWS/ETSs constructed as described below, and individual resistant clones were selected in DMEM containing 10% T-FBS and 200 to 300 μg/ml of Zeocin (Invitrogen). The Zeocin-resistant clones were expanded and tested for the induction of EWS/ETS expression upon the addition of tetracycline by use of reverse transcription-PCR (RT-PCR) as described below.

Plasmid construction. A gateway cassette (bases 1 to 1705) was amplified from pBLOCK-iT3-DEST (Invitrogen) by PCR, and the PCR product was inserted into the EcoRV site of pcDNA4-TO (Invitrogen) (termed pcDNA4-DEST). Since the type II EWS/FLI1 is a stronger transactivator than the type I product (32), we used the type II variant in the present study. EWS/ERG was isolated from W-ES, an EFT cell line, joining EWS exon 7 and ERG exon 9. Full-length EWS/FLI1 type II and EWS/ERG cDNAs were amplified from cDNAs prepared from NCR-EW2 and W-ES cells, respectively, by PCR as described below and cloned into the XmnI-EcoRV sites of pENTR11 (Invitrogen). The resulting pENTR11-EWS/ETSs were recombined with pcDNA4-DEST by use of LR recombination reaction as instructed by the manufacturer (Invitrogen) to construct the tetracycline-inducible EWS/ETS expression vector pcDNA4-EWS/ETSs.

Western blot analysis. UET-13 transfectants were cultivated with or without 3 μg/ml of tetracycline for 72 h. Western blot analysis was performed as previously described (37). Briefly, the cell lysates were prepared and separated on a 10% sodium dodecyl sulfate-polyacrylamide gel electrophoresis gel and transferred onto a polyvinylidene difluoride membrane. The membranes were blocked with 5% skimmed milk in phosphate-buffered saline (PBS) containing 0.01% Tween 20 (Sigma) and incubated with primary antibodies. As the primary antibodies, anti-Fli-1, anti-Erg-1/2/3 (Santa Cruz Biotechnology), and anti-actin (Sigma) were used. Horseradish peroxidase-conjugated anti-rabbit or anti-mouse immunoglobulin G (IgG) antibodies (DakoCytomation) were used as secondary antibodies. Blots were detected by chemiluminescence using an ECL Plus Western blotting detection system (GE Healthcare Bio-Science Corp.) and exposed to X-ray film (Kodak) for 5 to 30 min.

MTT assay and detection of apoptosis. Growth curves of UET-13 transfectants were determined using the 3-(4,5-dimethylthiazol-2-yl)-2,5-diphenyltetrazolium bromide (MTT) assay as described previously (18). The apoptosis was detected using an annexin V-fluorescein isothiocyanate (FITC) apoptosis detection kit (Biovision) according to the manufacturer's instructions and analyzed by flow cytometry (Cytomics FC500; Beckman Coulter).

Immunofluorescence analysis. After 1 week of culture in the absence or presence of tetracycline, UET-13 cells and the transfectants were harvested with 0.25% trypsin plus EDTA (IBL). The cells (2×10^5) were incubated with mouse monoclonal antibodies for 20 min. In the case of fluorescence-labeled antibodies, the cells were washed with PBS and then analyzed. In the case of primary unconjugated mouse antibodies, the cells were washed and then incubated with FITC-conjugated goat anti-mouse IgG antibody (Jackson ImmunoResearch Laboratories) for 20 min. Cell fluorescence was detected using a Cytomics FC500 instrument as described previously (27).

Antibodies against the following human antigens were used: CD10, CD13, CD14, CD29, CD34, CD40, CD44, CD45, CD49e, CD54, CD56, CD61, CD90, CD105, CD117, and CD166 from Beckman Coulter; CD73 from BD Biosciences-Pharmingen; CD55 from Abcam; CD59 from Cedarlane Laboratories; and CD133 and CD271 from Miltenyi Biotec GmbH.

Immunocytochemistry. Cells were grown on collagen type I-coated cover glasses (Iwaki). After 72 h with or without tetracycline, cells were fixed for 30 min in 4% paraformaldehyde and permeabilized in PBS containing 0.2% Triton X-100 (Sigma) for 30 min. Subsequently, they were washed with PBS and blocked in PBS containing 0.1% Triton X-100 and 1% bovine serum albumin (Sigma) for 30 min before being incubated with a monoclonal anti-CD99 antibody, i.e., 12E7 (1:100) (DakoCytomation) or O13 (1:200) (Thermo), and polyclonal anti-Fli-1 antibody (1:100) (Santa Cruz) for 1 h. Bound antibodies were visualized with appropriate secondary antibodies, i.e., Alexa Fluor 488 goat anti-mouse IgG (heavy plus light chains) highly cross-adsorbed and Alexa Fluor 546 goat anti-rabbit IgG (heavy plus light chains) highly cross-adsorbed (Invitrogen) for 1 h at 1:300. Nuclei were counterstained with 4′,6′-diamidino-2-phenylindole (DAPI) or propidium iodide (PI) (Sigma). For the visualization of whole cells, cells were treated with Celltracker Blue (Invitrogen) for 30 min and then fixed. Fluorescence was observed and analyzed using a confocal laser scanning microscope and image software (either FV500 from Olympus or LSM510 from Carl Zeiss). Precise measurements of cell size, nuclear size, and the nucleus-to-cytoplasm (N/C) ratio were performed using Image J (16).

RT-PCR analysis. Total RNA was extracted from cells by use of an RNeasy kit (Qiagen) and reverse transcribed using a first-strand cDNA synthesis kit (GE Healthcare Bio-Science Corp). RT-PCR was performed with a HotstarTaq master mix kit (Qiagen). As an internal control, human GAPDH cDNA was also amplified. The sequences of gene-specific primers for RT-PCR were as follows: for EWS/FLI1 (forward), 5′-ATGGCGTCCACGGATTACAGTACCT-3′; for EWS/FLI1 (reverse), 5′-GGGTCTTCTTTGACACTCAATCG-3′; for EWS/ERG (forward), 5′-ATGGCGTCCACGGATTACAGTACCT-3′; for EWS/ERG (reverse), 5′-TTAGTAGTAAGTGCCCAGATGAGAA-3′; for GAPDH (forward), 5′-CCACCCATGGCAAATTCCATGGCA-3′; and for GAPDH (reverse), 5′-TCTAGACGGCAGGTCAGGT/CCACC-3′. PCR products were electrophoresed with a 1% agarose gel and stained with ethidium bromide.

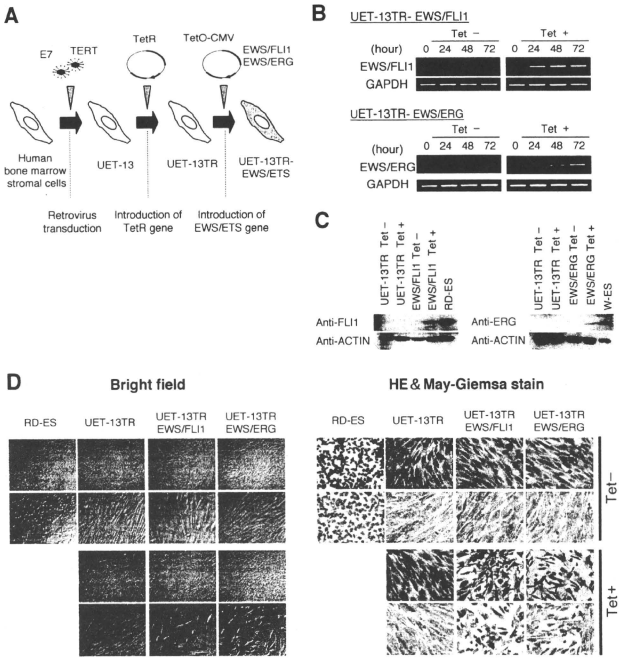

FIG. 1. The effect of EWS/ETS on the morphology of UET-13 cells. (A) The establishment of a tetracycline-inducible EWS/ETS expression system in UET-13 cells. CMV, cytomegalovirus. (B) Analyses for confirming the inducible expression of EWS/ETS genes. EWS/ETS mRNAs were detected in UET-13 transfectants UET-13TR-EWS/FLI1 and UET-13TR-EWS/ERG by RT-PCR. These cells were treated with or without 3 μg/ml of tetracycline (Tet) for the indicated periods. As an internal control, a human GAPDH gene was used. (C) Analyses for confirming the inducible expression of EWS/ETS proteins. The cells were treated as described for panel B and subjected to Western blotting for the detection of EWS/ETS proteins. The extracts of RD-ES and W-ES cells were also examined as positive controls. Membranes were reprobed with anti-actin antibody as a loading control. (D) Morphological change after tetracycline treatment of UET-13 transfectants. UET-13 cells and the transfectants were cultured in the absence or presence of tetracycline for 72 h and observed by light microscopy. Magnification, ×40 (top); ×200 (bottom). Cells were also examined using hematoxylin-eosin (HE) (top) and May-Giemsa (bottom) staining (magnification, ×200).

Real-time RT-PCR. Real-time RT-PCR was performed using TaqMan universal PCR master mix and TaqMan gene expression assays and an inventoried assay on an ABI Prism 7900HT sequence detection system (Applied Biosystems) according to the manufacturer's instructions. The human GAPDH gene was used as an internal control for normalization.

DNA microarray analysis. Total RNA isolated from cells was reverse transcribed and labeled using one-cycle target labeling and control reagents as instructed by the manufacturer (Affymetrix). The labeled probes were hybridized to the human genome U133 Plus 2.0 array (Affymetrix). The arrays were performed in a single experiment and analyzed using GeneChip operating software, version 1.2 (Affymetrix). Background subtraction, normalization, and principal component analysis (PCA) were performed by GeneSpring GX 7.3 software (Agilent Technologies). Signal intensities were prenormalized based on the median of all measurements on that chip. To account for the difference in detection efficiencies between the spots, prenormalized signal intensities on each gene were normalized to the median of prenormalized measurements for that gene. The data were filtered using the following steps. (i) Genes that were scored as absent in all samples were eliminated. (ii) Genes for which the signal intensities were lower than 100 were eliminated. (iii) Performing cluster analysis using filtering genes, we selected the genes that exhibited increased expression or decreased expression in tetracycline-treated cells. Accession numbers for the microarray data are given below.

Invasion assay. The invasion assay was performed using Matrigel (BD Bioscience) according to the previous description (34) with some modification. Polycarbonate filter inserts containing 8-μm pores (BD Falcon) were coated with 50 μl of a 6:1 mixture of culture medium and Matrigel and placed into 24-well culture plates containing DMEM supplemented with 10% T-FBS as chemoattractants. Cells (2.5×10^4) treated with or without tetracycline for 72 h were suspended in DMEM containing 0.01% T-FBS and plated on top of each filter insert. After 20 h in culture in the presence or absence of tetracycline, noninvading cells were removed from upper surface of the filter with a cotton swab. The invading cells on the lower surface of the filter were fixed with formalin, stained with hematoxylin-eosin, and counted in five fields per membrane with light microscopy. As a control, cells were also cultured on uncoated filter inserts. The invasion efficiency was presented as the ratio of the number of invading cells on Matrigel-coated inserts to that on uncoated inserts. Experiments were performed in triplicate, and the means with standard deviations of the values are shown in the graphs in Fig. 8.

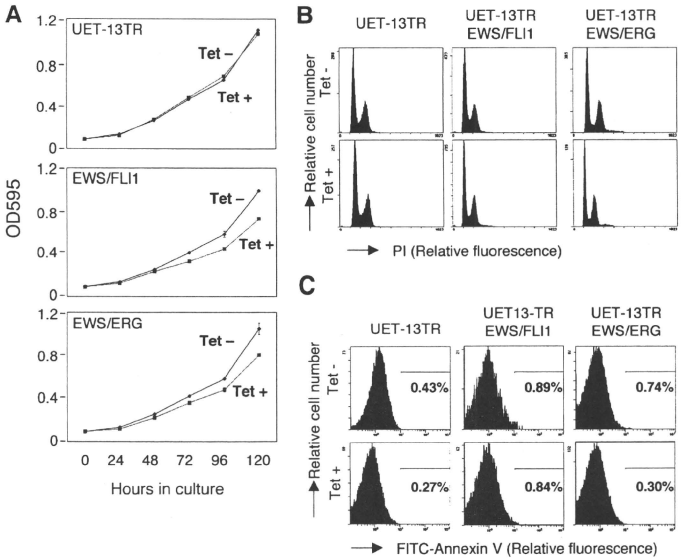

FIG. 2. Effects of EWS/ETS on cell growth in UET-13 cells. (A) Growth curve for UET-13 transfectants. Cells were seeded at 10^3/well and cultured as described for Fig. 1. The increase in cell number was analyzed by MTT assay. Values are means with the standard errors (SE) from three independent experiments. Diamond symbols indicate UET-13 transfectants in the absence of tetracycline (Tet); box symbols indicate UET-13 transfectants in the presence of tetracycline. (B) Cells were cultured as described for panel A in the absence or presence of tetracycline for 3 days and then stained with PI, and DNA contents were analyzed by flow cytometry (*x* axis, relative intensity of fluorescence; *y* axis, relative cell number). (C) Cells treated as described for panel B were stained with FITC-annexin V and analyzed.

Microarray data accession numbers. Microarray data have been deposited in the Gene Expression Omnibus database GEO (www.ncbi.nlm.nih.gov/geo) (accession numbers GSE8665 and GSE8596).

RESULTS

EWS/ETS expression results in morphological changes in UET-13 cells. To investigate how the expression of EWS/ETS affects human MPCs, we used UET-13 cells as a model of human MPCs and expressed EWS/FLI1 (UET-13TR-EWS/FLI1) and EWS/ERG (UET-13TR-EWS/ERG) in a tetracycline-inducible manner (Fig. 1A). As shown in Fig. 1B and C, we confirmed that the tetracycline treatment could induce EWS/ETS expression by RT-PCR analysis and Western blotting. The inducibility upon the addition of doxycycline was comparable to that upon the addition of tetracycline.

Using these cell systems, first we examined the effect of EWS/ETS expression on morphology in UET-13 transfectants. When tetracycline was added to the culture, the morphologies of both UET-13TR-EWS/FLI1 and UET-13TR-EWS/ERG cells were dramatically changed (Fig. 1D). Tetracycline-treated UET-13TR-EWS/ETS cells consisted of a mixture of small round-to-polygonal cells and short spindle cells. The cell morphology resembled that of EFT cell lines. To assess the reproducibility of this phenotypic change, other UET-13TR-EWS/ETS clones were examined, and similar morphological changes were observed. Since tetracycline treatment did not affect the morphology of UET-13TR cells (Fig. 1D), it was suggested that the morphological alteration in UET-13 cells from a mesenchymal cell shape to small round cells, one of the characteristics of EFT, can be attributed to EWS/ETS expression.

EWS/ETS expression inhibits cell growth in UET-13 cells. Next, the effect of EWS/ETS expression on the growth of UET-13 cells was analyzed. As shown in Fig. 2A, an MTT assay revealed that the addition of tetracycline had no effect on the growth of UET-13TR cells but slightly inhibited that of UET-13TR-EWS/ETS cells. We also assessed the cell growth of UET-13 transfectants after tetracycline addition by cell counting and obtained results well in accord with those from the MTT assay (data not shown). To determine the mechanism of this inhibition, DNA content and the binding of annexin V to UET-13 transfectants were examined. No significant increase in either sub-G_1-phase cells (Fig. 2B) or annexin V binding cells (Fig. 2C) was detected, suggesting that EWS/ETS-mediated growth inhibition in UET-13 cells was not due to the activation of an apoptotic pathway. Moreover, no significant decrease in S-G_2-phase cells was observed (Fig. 2B).

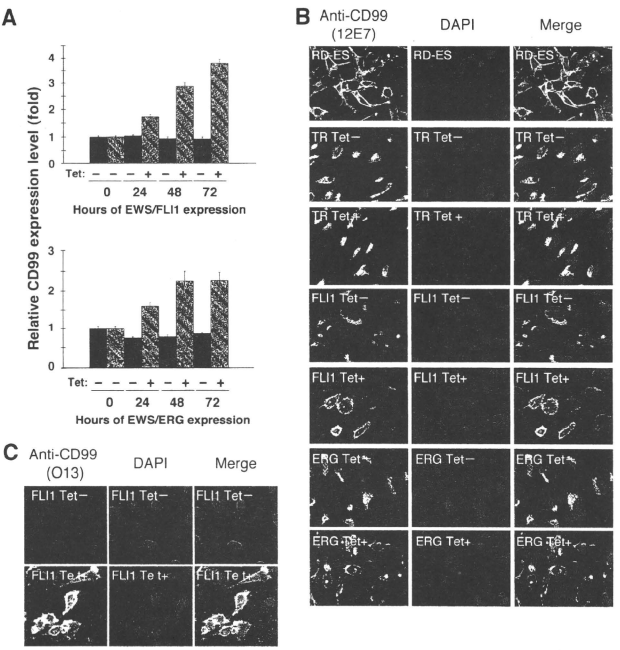

FIG. 3. Effects of tetracycline-mediated EWS/ETS expression on the expression and distribution of CD99 in UET-13 cells. (A) Relative CD99 levels in UET-13 transfectants in the absence or presence of tetracycline (Tet). UET-13 transfectants were treated with or without 3 μg/ml of tetracycline for the indicated periods. Real-time RT-PCR was performed to investigate the expression pattern of CD99. Signal intensities of CD99 were normalized using those of a control housekeeping gene (human GAPDH gene). Data are relative values with standard deviations from triplicate wells and are normalized to the mRNA level at 0 h, which is arbitrarily set to 1 in the graphical presentation. (B and C) Immunocytostaining of CD99 in UET-13 transfectants. Cells were cultured on coverslips in the absence or presence of tetracycline for 72 h and then stained with anti-CD99 antibody 12E7 (B) or O13 (C) as described in Materials and Methods. RD-ES cells were also examined as a positive control. For the staining of nuclei, DAPI was used.

Effect of EWS/ETS on CD99 expression in UET-13 cells. The p30/32MIC-2 gene product, CD99, is a cell surface glycoprotein expressed in EFT with a strong membranous staining pattern and thus constitutes a useful marker for EFT (2, 30). Knowing the dramatic change of morphology in UET-13 cells, we next investigated the mRNA level of CD99 in tetracycline-treated and untreated UET-13 transfectants by quantitative real-time RT-PCR. CD99 levels were clearly elevated by tetracycline treatment in both UET-13TR-EWS/FLI1 and UET-13TR-EWS/ERG cells in a time-dependent manner (Fig. 3A).

We also examined the protein expression of CD99 by immunostaining using 12E7 antibody, which is most widely used as an anti-CD99 antibody. An EFT cell line, RD-ES, showed strong membranous staining of CD99 (Fig. 3B), while neither UET-13TR cells nor UET-13 cells had such a staining. Of note is the fact that although 12E7 reactivity was observed only in the cytoplasm in perinuclear regions in both UET-13TR (Fig. 3B) and UET-13 (data not shown) cells, this antibody is well known to cross-react with a cytoplasmic protein not yet characterized. Since another anti-CD99 antibody, O13, did not react with either UET-13TR (Fig. 3C) or UET-13 (data not shown) cells, we concluded that the perinuclear staining of 12E7 mentioned above was a cross-reaction with unrelated proteins.

In the absence of tetracycline, both UET-13TR-EWS/FLI1 and UET-13TR-EWS/ERG cells were also negative with anti-CD99 antibodies (a pattern designated $CD99^-$), similar to UET-13 cells. Surprisingly, however, tetracycline induced a membranous staining pattern (designated $CD99^+$) in UET-13TR-EWS/FLI1 and UET-13TR-EWS/ERG cells, and some $CD99^+$ cells had irregularly contoured nuclei (Fig. 3B). The same results were observed with another anti-CD99 antibody, O13 (Fig. 3C), indicating that the membranous staining observed for UET-13 transfectants with the anti-CD99 antibodies

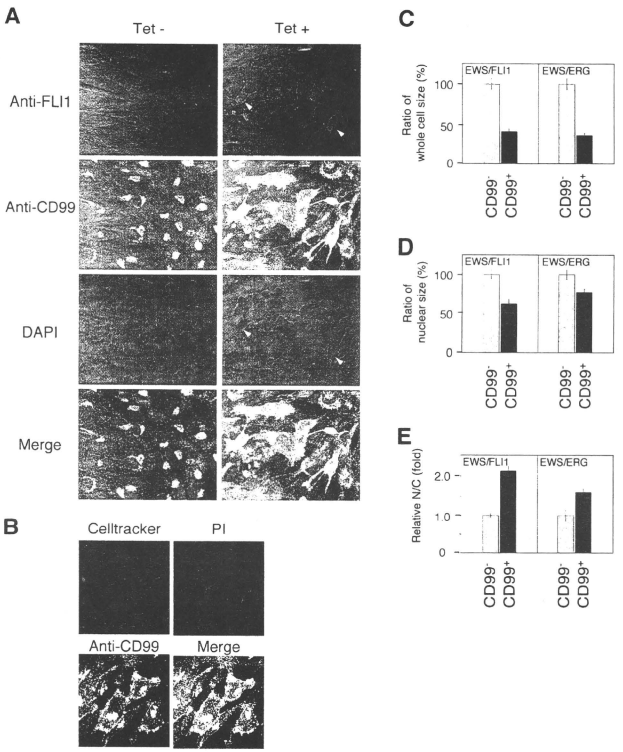

FIG. 4. EWS/ETS expression, alteration of CD99 distribution, and cell morphological changes in UET-13 cells. (A) Immunofluorescence studies using anti-Fli1 (red), anti-CD99 (green), and DAPI (blue). UET-13TR-EWS/FLI1 cells were cultured on coverslips in the absence or presence of tetracycline (Tet) for 72 h and then stained as described in Materials and Methods. White arrowheads indicate $CD99^+$ cells that have a strong staining pattern with anti-Fli1 antibodies and also have remarkable CD99 expression and morphological features. (B) Immunofluorescence analysis by triple staining with whole cells (Celltracker; blue), CD99 (anti-CD99; green), and nuclei (PI; red). UET-13TR-EWS/FLI1 cells were cultured as described for panel A and then stained as described in Materials and Methods. (C to E) Measurements of whole-cell size (C), nuclear size (D), and N/C ratio (E) in tetracycline-treated UET-13 transfectants. UET-13TR-EWS/FLI1 and UET-13TR-EWS/ERG cells were cultured on coverslips in the presence of tetracycline for 72 h and then stained as described in Materials and Methods. These samples were analyzed by the image analysis software Image J ($n = 50$). (C and D) Data are relative values with the SE and are normalized to the size of $CD99^-$ cells, which is arbitrarily set to 100. (E) Data are relative values with the SE and are normalized to the size of $CD99^-$ cells, which is arbitrarily set to 1.

was really CD99 derived. Despite the fact that cells were single colony derived, there was a heterogeneous response to tetracycline treatment in UET-13TR-EWS/FLI1 and UET-13TR-EWS/ERG cells, but most of the $CD99^+$ cells had a small round morphology, one of the characteristics of EFT. To assess the correlation between EWS/FLI1 expression and the change of the CD99 expression pattern, we performed immunofluorescence studies using anti-Fli1 and anti-CD99 antibodies. As shown in Fig. 4A, tetracycline treatment induced a marked enhancement of nuclear staining with anti-Fli1 antibodies in a large number of UET-13TR-EWS/FLI1 cells, indicating the induction of EWS/FLI1 proteins. Furthermore, we observed that the cells with a strong signal for Fli1 tended to reveal a membranous staining pattern with anti-CD99 antibodies and a small round morphology (Fig. 4A). To further verify the correlation between CD99 expression pattern and cell morphology, we estimated the size of cells by triple staining using Celltracker Blue, PI, and anti-CD99 antibody (Fig. 4B). As

TABLE 2. Immunophenotypic characterization of UET-13 transfectants and EFT cells

MPC status[a]	CD marker	Result for[b]: UET-13	UET-13TR		UET-13TR-EWS/FLI1		UET-13TR-EWS/ERG		RD-ES	EFT status[c]	SK-ES1
		Tet$^-$	Tet$^+$	Tet$^-$	Tet$^+$	Tet$^-$	Tet$^+$				
M+	CD29	+	+	+	+	+	+	+	+	+	
M+	CD59	+	+	+	+	+	+	+	+	+	
M+	CD90	+	+	+	+	+	+	+	+	+	E+
M+	CD105	+	+	+	+	+	+	+	+	+	
M+	CD166	+	+	+	+	+	+	+	+	+	
M+	CD44	+	+	+	+	+	+	+	−	−	
M+	CD73	+	+	+	+	+	+	+	−	−	
M+	**CD10**	**+**	**+**	**+**	**+**	**Down**	**+**	**Down**	**−**	**−**	
M+	**CD13**	**+**	**+**	**+**	**+**	**Down**	**+**	**Down**	**−**	**−**	
M+	**CD49e**	**+**	**+**	**+**	**+**	**Down**	**+**	**Down**	**+**	**−**	
M+	**CD61**	**+**	**+**	**+**	**+**	**Down**	**+**	**Down**	**−**	**−**	
M+	**CD55**	**+**	**+**	**+**	**+**	**Down**	**+**	**+**	**+**	**−**	
M+	**CD54**	**−**	**−**	**−**	**−**	**Up**	**−**	**Up**	**+**	**+**	E+
M(−)	**CD117**	**−**	**−**	**−**	**−**	**Up**	**−**	**Up**	**+**	**+**	E+
M+/−	**CD271**	**−**	**−**	**−**	**−**	**Up**	**−**	**Up**	**+**	**+**	E+
	CD40	−	−	−	−	−	−	−	+	+	E+
	CD56	−	−	−	−	−	−	−	+	+	E+
M(−)	CD133	−	−	−	−	−	−	−	+	+	
M(−)	CD14	−	−	−	−	−	−	−	−	−	
M(−)	CD34	−	−	−	−	−	−	−	−	−	
M(−)	CD45	−	−	−	−	−	−	−	−	−	

[a] M(−), negative for MPCs; M+/−, positive for BM-derived MPCs but negative after in vitro culture; M+, positive for MPCs.
[b] +, most cells positive; −, negative; Up, up-regulated by tetracycline treatment; Down, down-regulated by tetracycline treatment. Boldface indicates the antigens the immunophenotypes of which were changed in favor of EFT. Tet$^-$, tetracycline negative; Tet$^+$, tetracycline positive.
[c] E+, positive for EFTs.

presented in Fig. 4C and D, the results clearly showed that the majority of CD99$^+$ cells were significantly smaller in both whole-cell size and nuclear size than the CD99$^-$ cells. Moreover, CD99$^+$ cells also had a substantially increased N/C ratio (Fig. 4E). These results indicated that EWS/ETS expression promoted CD99 expression in UET-13 cells, and CD99 expression status is correlated with the degree of morphological change.

EWS/ETS expression altered the immunophenotype of UET-13 cells. Human MPCs reveal a characteristic expression of several surface antigens and can be identified on the basis of the reactivity with a set of monoclonal antibodies against CD antigens (25, 42). On the other hand, some CD antigens are characteristically expressed on EFT cells (17, 28, 33). Using the combinations of these antibodies listed in Table 2, which are useful for the immunodetection of either MPCs or EFT cells, we further examined whether EWS/ETS expression affects the immunophenotype of UET-13 cells and compared its effect with that on the immunophenotype of EFT cell lines (Table 2 and Fig. 5). As shown in Table 2, UET-13 cells express most of the human primary MPCs markers. Some of the antigens expressed in MPCs, namely, CD29, CD59, CD90, CD105, and CD166, were also found to be expressed in EFT cell lines, but others, namely, CD10, CD13, CD44, CD61, and CD73, were not. In contrast, antigens recognized to be present in EFT cells, including CD40, CD56, and CD133, were absent from UET-13 cells. Interestingly, when the effect of tetracycline-mediated EWS/ETS expression on the immunophenotype of UET-13 cells was tested, levels of some of the antigens present in UET-13 cells, such as CD10, CD13, and CD61, were found to be decreased (Fig. 5). In contrast, some of the markers found in EFT cells, i.e., CD54, CD117, and CD271, became positive in UET-13TR-EWS/ETS cells after tetracycline treatment. Because UET-13TR cells did not show such immunophenotypic change upon treatment with tetracycline, these results indicated that, at least in part, the immunophenotype of UET-13 cells was changed in favor of EFT in the presence of EWS/ETS.

EWS/ETS in UET-13 cells modulates EFT-like gene expression. To further examine the molecular mechanism of EWS/ETS-dependent cellular modulation in human mesenchymal progenitor background, we performed DNA microarray-based expression profiling using the Affymetrix human genome U133 Plus 2.0 array. As a first step to this approach, we validated our experimental systems by analyzing the sequential changes of known EWS/ETS target genes, i.e., inhibitor of differentiation 2 (ID2) (14, 39), NK2 transcription factor related, locus 2 (NKX2.2) (9, 48), and insulin-like growth factor binding protein 3 (IGFBP3) (41). Consistent with previous reports, levels of ID2 and NKX2.2 increased with the expression of EWS/ETS in a time-dependent manner, whereas the expression level of IGFBP3 decreased (Fig. 6A). Employing the same procedure, we also examined whether the change of surface antigen expression was regulated at the transcriptional level and determined the mRNA expression levels of some surface antigens in UET-13 transfectants with or without tetracycline treatment. In accordance with the results of immunocytometric and immunohistological experiments, the mRNA expression levels of CD10, CD13, CD49e, and CD61 were decreased, while those of CD54, CD99, CD117, and CD271 were markedly increased in tetracycline-treated UET-13TR-EWS/ETS cells (Fig. 6B and C), indicating that the expression of these antigens is

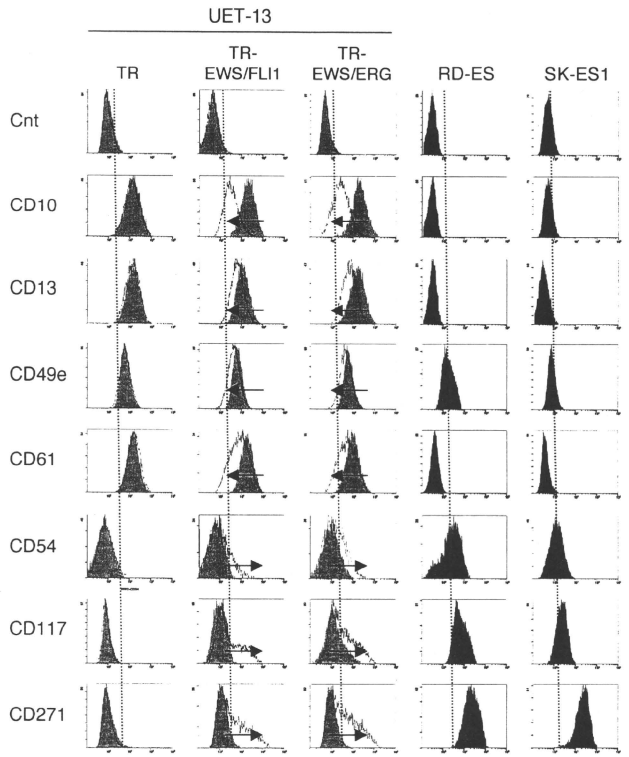

FIG. 5. Immunophenotypic change on induction of EWS/ETS expression in UET-13 cells. UET-13 transfectants were cultured with or without 3 μg/ml of tetracycline for 1 week and flow cytometric analyses were performed by using a set of antibodies as indicated. The histograms of UET-13 transfectants with (empty) and without (gray) tetracycline treatment were overlaid. Dotted lines indicate fluorescence intensities in negative control panels (Cnt). Arrows indicate the immunophenotypic change caused by tetracycline. The immunophenotypes of the EFT cell lines RD-ES and SK-ES1 were also examined.

controlled at the transcriptional level in the presence of EWS/ETS.

We next investigated the candidate genes whose expression is regulated by EWS/ETS in human MPCs. First, we selected the genes with up-regulated or down-regulated expression by EWS/ETS induction using gene cluster analysis (Fig. 7A; UET-13TR-EWS/FLI1 up, 4,294 probes; down, 4,103 probes; UET-13TR-EWS/ERG up, 3,358 probes; down, 3,705 probes). To reduce the number of the candidate genes, we selected up-regulated genes that are expressed in tetracycline-treated cells at least 1.5-fold higher than in untreated cells (UET-13TR-EWS/FLI1, 1,137 probes; UET-13TR-EWS/ERG, 835 probes). Similarly, the down-regulated genes that are expressed in tetracycline-treated cells at least 0.75-fold lower than in untreated cells (UET-13TR-EWS/FLI1, 1,803 probes; UET-13TR-EWS/ERG, 773 probes). By selecting common probes in both cells, we finally identified a group of candidate genes significantly controlled by EWS/ETS induction in the human mesenchymal progenitor background. Since microarray analysis was performed as a global screening in a single experiment, it is likely that there is a fair bit of noise in the derived gene profiles due to the lack of replicate data. This may account in part for the limited overlap between the profiles induced by EWS-FLI1 and EWS-ERG, whereas we still identified 349 probes of common up-regulated genes and 293 probes of common down-regulated genes (see the supplemental material). In addition to the EFT-specific genes mentioned above, these contained those previously described as EFT-specific genes, such as those for OB-cadherin/cadherin-11 (31), Janus

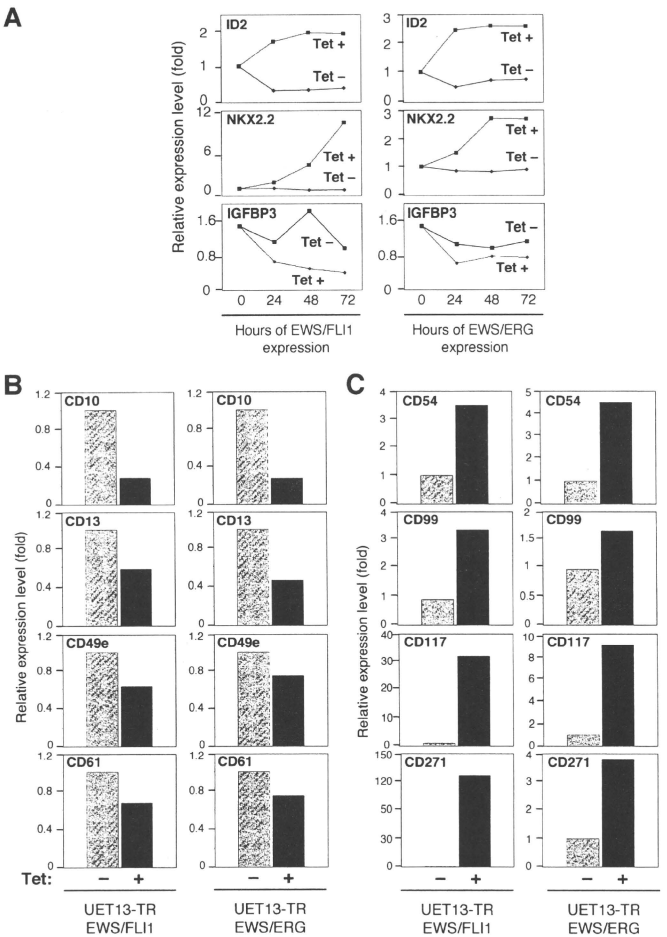

FIG. 6. The change of expression profile on induction of EWS/ETS in UET-13 cells. UET-13TR-EWS/FLI1 and UET-13TR-EWS/ERG cells were cultured in the absence or presence of tetracycline (Tet) for the indicated periods and analyzed using the Affymetrix human genome U133 Plus 2.0 array as described in Materials and Methods. (A) The sequential changes of ID2, NKX2.2, and IGFBP3 mRNA levels in UET-13 transfectants upon treatment with or without tetracycline. Diamond symbols indicate UET-13 transfectants in the absence of tetracycline; box symbols indicate UET-13 transfectants in the presence of tetracycline. (B and C) Microarray studies for the determination of expression profiles of surface antigens in UET-13 transfectants. UET-13 transfectants were treated with or without 3 μg/ml of tetracycline for 72 h. mRNA levels were determined with the Affymetrix human genome U133 Plus 2.0 array.

kinase 1 (JAK1) (49), keratin 18, and six-transmembrane epithelial antigen of the prostate (STEAP) (22). The expression pattern of these genes (642 probes) in UET-13 transfectants in the absence or presence of tetracycline is shown in the gene cluster in Fig. 7B. The expression of these genes was indeed changed significantly after EWS/ETS expression in both cells. They included genes associated with signal transduction (such as those for epidermal growth factor receptor, FAS [CD95], and fibroblast

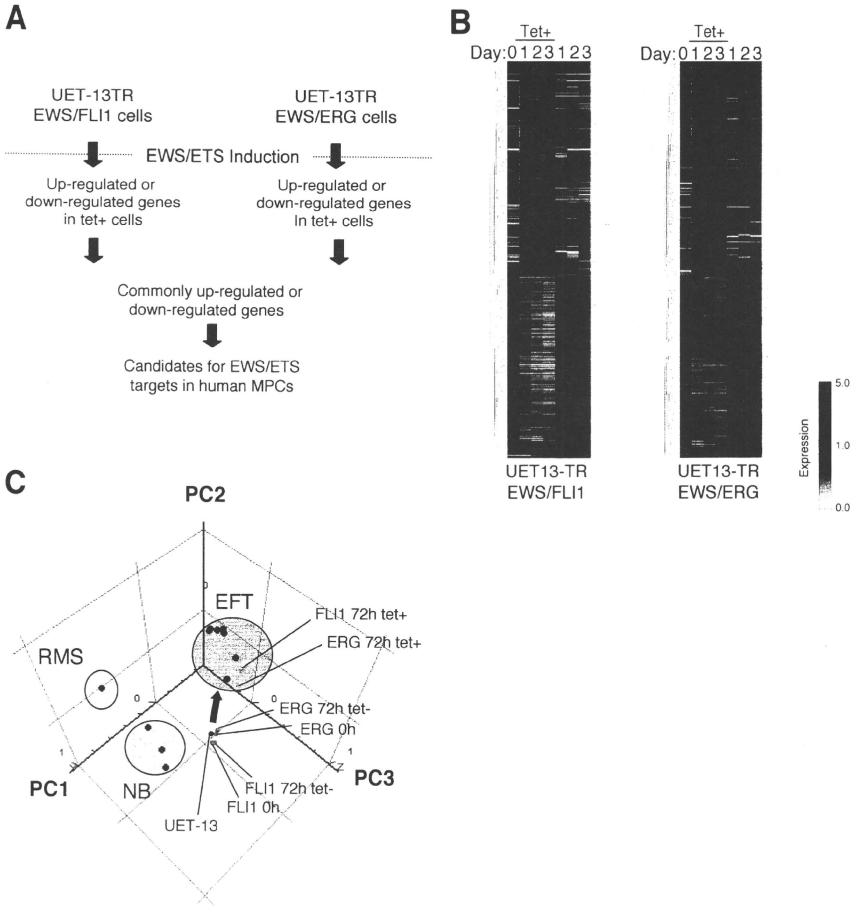

FIG. 7. Identification of candidates for the target of EWS/ETS in human MPCs by use of a microarray. UET-13TR-EWS/FLI1 and UET-13TR-EWS/ERG cells were cultured as described for Fig. 6 and analyzed using the Affymetrix human genome U133 Plus 2.0 array as described in Materials and Methods. (A) Scheme for the analysis of microarray data. (B) Gene cluster analysis of UET-13 transfectants in the absence or presence of tetracycline by use of 642 candidate genes for targets of EWS/ETS in human MPCs. (C) Visualization of sequential change by the gene expression profile in UET-13 transfectants following tetracycline-mediated EWS/ETS expression based on a PCA of 642 candidate genes. Deep blue plots indicate UET-13 cells. Light blue plots indicate UET-13 transfectants in the absence of tetracycline for 72 h. Yellow plots indicate UET-13 transfectants in the presence of tetracycline for 72 h. The pink circle indicates EFT cell lines expressing EWS/FLI1 (purple plots), EWS/ERG (red plot), and EWS/E1AF (light green plot). The light blue circle with blue plots indicates NB cell lines. The yellow circle with an orange plot indicates a rhabdomyosarcoma (RMS) cell line. Cutoff induction and repression levels are 1.5-fold and 0.75-fold, respectively. Tet, tetracycline.